Sound source identification at tire-pavement interactions – a preliminary study

Jonathan Nowak[1], Manfred Kaltenbacher[2]
[1] TU Wien, Vienna, Austria, Email: jonathan.nowak@tuwien.ac.at
[2] TU Graz, Graz, Austria, Email: manfred.kaltenbacher@tugraz.at

Introduction

Tire noise has become a highly relevant topic in research and practice since tire-pavement interactions are main sound sources in the middle speed range of passenger cars besides noise emitted by the engine and aerodynamic sound sources. Tire noise is even more relevant when thinking of electric vehicles, since there is almost no engine noise. Common methods for measuring tire and road noise are mainly based on norms not considering localization of sound sources due to the tire-pavement interaction.

With the goal of identifying all relevant sound sources at a rolling tire using a trailer equipped with multiple microphones, a preliminary study was performed. In this study a stationary model of a trailer for passenger cars was constructed. This stationary trailer is equipped with sound absorbers and multiple distributed microphones for performing different sound source localization algorithms, such as beamforming based algorithms and a new method solving the inverse problem of matching sound pressure measurements and finite element computations. With the latter method the boundary conditions of the given measurement setup can be taken into account. Details about this inverse scheme and sound source localization results can be found in [1, 2, 3]. This method requires characterization of the measurement environment's material parameters. In this contribution the characterization process of the stationary trailer and the validation of the FE model is presented.

Setup

In this section the setup of the preliminary study is presented. Figure 1 shows the stationary model of a vehicle trailer of which the boundary conditions shall be determined. The wooden box measures approximately $2.3 \times 2 \times 1.5\,\mathrm{m}$ (L × W × H) and is equipped with acoustic absorbers inside, micro perforated plates (MPP) at the side walls as well as the ceiling and porous absorbers in the corners. The micro perforated plates are made of aluminum and have very small slits. In combination with a backing air volume and a sound hard termination (wooden wall) these plates can be used as acoustic absorbers (micro perforated absorbers, MPA). With the length of the backing volume, the peak frequencies concerning sound absorption can be adjusted. In this setup two layers of MPPs are used to achieve a more broadband sound absorption. For this setup the MPPs and back volumes were configured such that high sound absorption is achieved for approximately $300\,\mathrm{Hz} \leq f \leq 2000\,\mathrm{Hz}$. For further details on micro perforated plates see [4, 5].

Since there is no rolling tire present, a loudspeaker and electret microphones are used as sound source and for measuring the acoustic pressure, respectively.

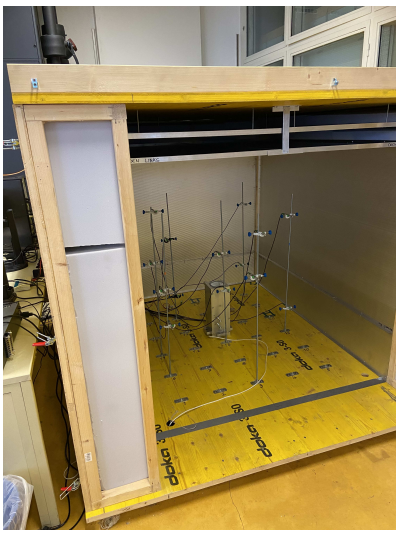

Figure 1: Stationary model of a vehicle trailer with micro perforated plates and porous absorbers for sound absorption.

Determining boundary conditions

Common methods for sound localization such as beamforming based algorithms or acoustic near-field holography usually assume free field radiation. In most cases these conditions do not fully apply in real world scenarios as sound is typically partially reflected at walls or scatterers. The mentioned inverse method overcomes this restriction as it is able to take the real measurement environment into account and e. g. acoustic absorbers can be modeled in the finite element computation.

We model regions with sound absorption based on Biot's theory [6] as an equivalent (complex) fluid. Acoustic absorbers such as e. g. poroelastic materials consist of a skeleton and a fluid part. If the skeleton can be modeled as rigid, waves in the solid part can be neglected and the material can be modeled as equivalent fluid which is responsible for dissipation of acoustic energy. This dissipation can be illustrated when we consider the 1D solution of the wave equation in frequency domain (Helmholtz equation)

$$\nabla^2 \widetilde{p}_\mathrm{a}(\boldsymbol{x}, \omega) + k^2 \widetilde{p}_\mathrm{a}(\boldsymbol{x}, \omega) = 0\,, \tag{1}$$

with the complex valued acoustic pressure $\widetilde{p}_\mathrm{a}$ and the wave number k which is defined as

$$k = \frac{\omega}{c} = \omega \sqrt{\frac{\varrho}{K}}\,. \tag{2}$$

In (1) ω denotes the angular frequency, c the speed of sound, ϱ the density and K the bulk modulus. The 1D solution of (1) for a propagating wave in an arbitrary direction r is given by

$$\widetilde{p}_\mathrm{a} = \hat{p}\,\mathrm{e}^{-\mathrm{j}kr}\,, \tag{3}$$

with the amplitude $\hat{p}$ of the propagating wave. When modeling sound absorption, the density and bulk modulus and therefore also the wave number is assumed to be complex valued

$$\widetilde{k} = \omega\sqrt{\frac{\widetilde{\varrho}}{\widetilde{K}}} = k_\mathrm{Re} - \mathrm{j}\,k_\mathrm{Im} \tag{4}$$

and we can see the damping effect in the 1D solution of the Helmholtz equation

$$\widetilde{p}_\mathrm{a} = \hat{p}\,\mathrm{e}^{-\mathrm{j}\widetilde{k}r} = \hat{p}\,\mathrm{e}^{-\mathrm{j}k_\mathrm{Re}r}\underbrace{\mathrm{e}^{-k_\mathrm{Im}r}}_{\text{damping}}\,. \tag{5}$$

The complex valued density and bulk modulus can be gained via the transfer matrix computed with the four microphone method in an impedance tube, see [7]. As the MPA needs a sound hard termination, this method cannot be applied. Therefore, the two-microphone method was used in order to measure the reflection coefficient $\widetilde{r}$, which is the ratio between the reflected and incoming sound pressure when a sound wave impinges on the absorber. Subsequently, a suitable material model is used to calculate the complex density $\widetilde{\varrho}$ and bulk modulus $\widetilde{K}$. The material model parameters are fitted such that the difference between measured $\widetilde{r}_\mathrm{meas}$ and calculated reflection coefficient $\widetilde{r}_\mathrm{calc}(\widetilde{\varrho}, \widetilde{K})$ is minimized. It has to be mentioned, that measurements in an impedance tube assume plane waves. Hence, absorbers can show different absorption and reflection behavior in an impedance tube than when applied in a general sound field, e. g. a diffuse field.

Material model

There are various material models for sound absorbing materials, for example the Delany-Bazely-Miki (DBM) [8] or Johnson-Champoux-Allard-Lafarge (JCAL) [9] model. For modeling the MPA the latter model is used, which is a semi empirical model and uses six model parameters a_i: the air flow resistivity σ, porosity ϕ, tortuosity in the high frequency limit α_∞, viscous characteristic length Λ, thermal characteristic length Λ' and static thermal permeability k_0'. For detailed explanations and formulae see [9].

Results for material parameters' fitting

As previously mentioned, the material model parameters a_i are varied such that the difference between measured and calculated reflection coefficient $\widetilde{r}$ is minimized

$$\min_{a_i} ||\widetilde{r}_\mathrm{calc}(a_i) - \widetilde{r}_\mathrm{meas}||\,. \tag{6}$$

In (6) $\widetilde{r}_\mathrm{calc}$ is a function of the surface impedance $\widetilde{Z}_\mathrm{s}(\widetilde{\varrho}, \widetilde{K})$, $\widetilde{\varrho} = \widetilde{\varrho}(a_i)$ and $\widetilde{K} = \widetilde{K}(a_i)$ of the considered absorber

$$\widetilde{r}_\mathrm{calc} = \frac{\widetilde{Z}_\mathrm{s} - \varrho_0 c_0}{\widetilde{Z}_\mathrm{s} + \varrho_0 c_0} \tag{7}$$

and ϱ_0 and c_0 are the density and speed of sound for air.

In fig. 2 one can see the measured and calculated reflection coefficient $\widetilde{r}$ of a micro perforated absorber (MPA) with two spaced layers of MPPs. The measurement was performed in an impedance tube and the JCAL model was used to describe the acoustic properties of this absorber. The model parameters were fitted to the measurement for frequencies $300 \leq f \leq 700\,\mathrm{Hz}$, marked in light gray in fig. 2. This frequency band is shifted when simulating higher frequencies. One can see very good agreement between the measured and fitted reflection coefficient in the marked frequency band. The obtained values for the complex valued density and bulk modulus serve as input parameters for the finite element computation.

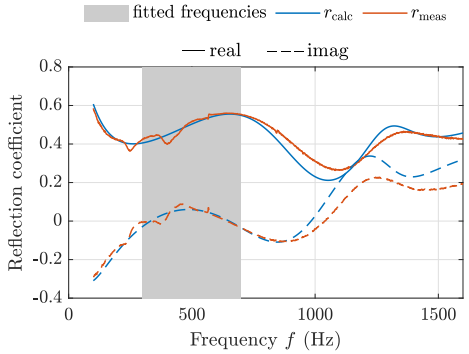

Figure 2: Measured and calculated reflection coefficient of an MPA with JCAL material model, fitted to measurement for $300 \leq f \leq 700\,\mathrm{Hz}$.

Finite element model

We solve (1) with the finite element method to obtain the acoustic pressure $\widetilde{p}_\mathrm{a}$ in frequency domain. In doing so, we first derive the weak formulation of (1) by multiplying it with an appropriate test function φ and integrating over the whole computational domain and applying Gauss's theorem. The weak form reads as

$$\int_\Omega \left(\nabla\widetilde{p}_\mathrm{a}\cdot\nabla\varphi - k^2\widetilde{p}_\mathrm{a}\varphi\right)\,\mathrm{d}\boldsymbol{x} = \int_{\partial\Omega}\varphi\nabla\widetilde{p}_\mathrm{a}\cdot\boldsymbol{n}\,\mathrm{d}s \qquad \forall\varphi\in V, \tag{8}$$

with the function space V for the test functions. The normal derivative of the acoustic pressure in the integrand on the right hand side of (8) can be expressed with the linearized conservation of momentum as

$$\nabla\widetilde{p}_\mathrm{a}\cdot\boldsymbol{n} = \widetilde{p}_\mathrm{a,n} = -\mathrm{j}\,\omega\rho_0\widetilde{v}_\mathrm{n}, \tag{9}$$

with the acoustic normal velocity $\widetilde{v}_\mathrm{n}$. Since the acoustic excitation is performed with a loudspeaker, prescribing $\widetilde{v}_\mathrm{n}$ is suitable to model the moving membrane.

In order to find the correct excitation in the simulation, laser scanning measurements of the loudspeaker membrane were performed. The loudspeaker used, showed a rigid body motion for frequencies $f \lesssim 1200\,\mathrm{Hz}$. Thus, the

loudspeaker was modeled as a plate with a single acoustic normal velocity amplitude and phase. At higher frequencies higher order modes come into effect, therefore results for $f > 1200$ should be treated with caution.

Computational mesh

The discretization of the computational domain is shown in fig. 3, the absorbers are depicted in yellow (porous absorber) and blue (MPP). The size of the hexagonal elements of first order is $h = 17\,\text{mm}$. Therefore, approximately 20 elements per wavelength at a frequency of 1000 Hz are used.

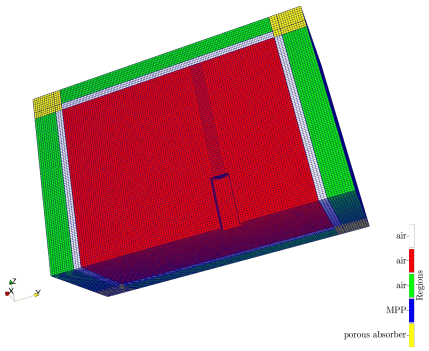

(a) Discretized stationary trailer.

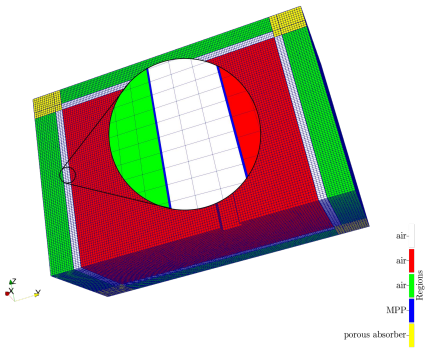

(b) Detail: micro perforated plates (blue).

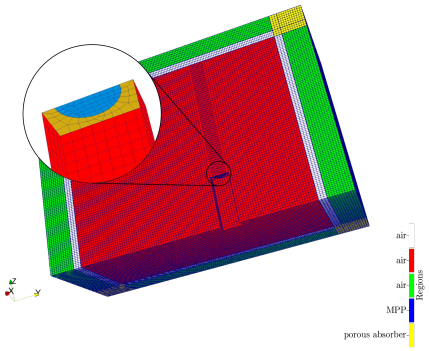

(c) Detail: membrane of loudspeaker (light blue).

Figure 3: Mesh for FE computation.

Results comparison measurement and simulation

The following results were performed with our in-house, open source finite element solver openCFS [10]. The acoustic pressure was measured inside the stationary trailer with electret microphones at 14 positions (see fig. 4) and the simulated sound pressure was evaluated at the same positions. The amplitude and phase of the membrane's acoustic normal velocity was recorded and prescribed in the simulation accordingly in a weak sense, see (8) and (9).

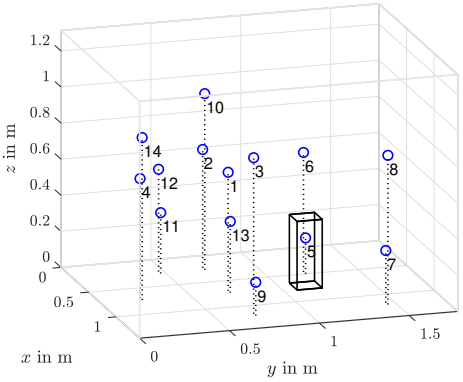

Figure 4: Microphone positions.

In the following a comparison between measured and simulated pressure in amplitude (fig. 5) and phase (fig. 6) at different frequencies is presented. The acoustic pressures and phases are plotted over the microphone numbers (fig. 4). It has to be noted that since we measure the acoustic particle velocity at the loudspeaker membrane synchronously with the acoustic pressure, we are able to simulate the acoustic pressure without any scaling.

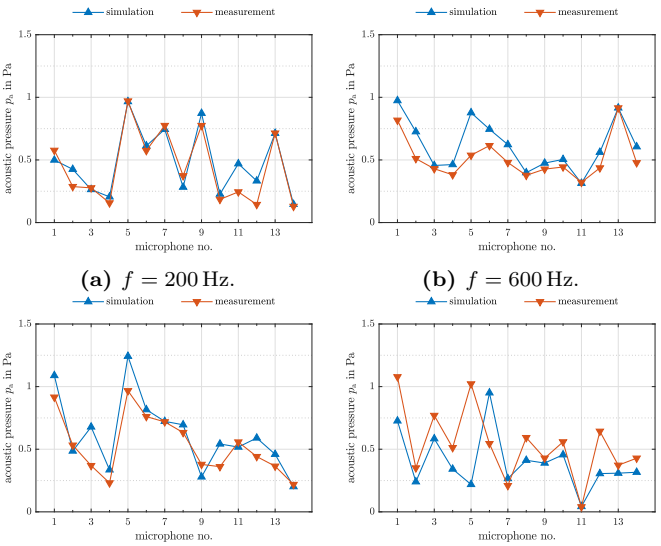

(a) $f = 200\,\text{Hz}$. **(b)** $f = 600\,\text{Hz}$.

(c) $f = 1000\,\text{Hz}$. **(d)** $f = 1600\,\text{Hz}$.

Figure 5: Comparison of the amplitude of measured and simulated acoustic pressure inside the stationary trailer, plotted over the corresponding microphone number.

This comparison shows good agreement between measurement and simulation in both amplitude and phase, especially in the lower frequency range. For $f = 1600\,\text{Hz}$ the deviation is higher. Again it has to be mentioned that the material properties were determined with plane

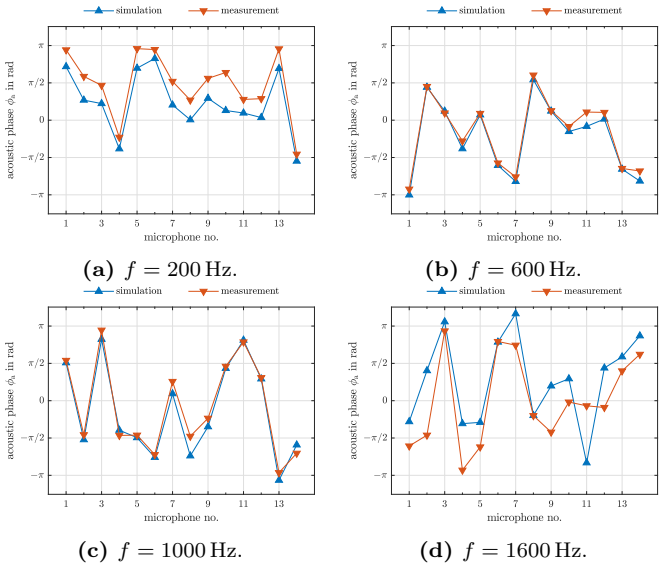

(a) $f = 200\,\mathrm{Hz}$. **(b)** $f = 600\,\mathrm{Hz}$.

(c) $f = 1000\,\mathrm{Hz}$. **(d)** $f = 1600\,\mathrm{Hz}$.

Figure 6: Comparison of the phase of measured and simulated acoustic pressure inside the stationary trailer, plotted over the corresponding microphone number.

wave excitation but the real sound field is scattered and therefore sound waves arrive at arbitrary angles at the absorbers. The higher deviation at higher frequencies is on the one hand due to the higher mode motion of the membrane. On the other hand the wave length decreases with increasing frequency, which means that length dimensions such as microphone positions, dimensions of the box and MPP positions become more important. In other words the order of magnitude of possible small errors e. g. in determining the microphone positions become similar to the order of magnitude of the wave length with increasing frequency.

Further, we just calibrated the electret microphones at the single frequency of 1 kHz. So it is possible that some microphones show different sensitivities at other frequencies and therefore don't measure the sound pressure amplitude as precise.

Outlook

Since the boundary conditions of the given setup are determined and validated, the next step is to apply the inverse scheme for sound source identification inside the stationary trailer and compare it to other sound source localization methods such as beamforming based algorithms and acoustic near field holography. Further, we will apply the mentioned methods to a real vehicle trailer and perform sound localization at the rolling tire.

References

[1] M. Kaltenbacher, B. Kaltenbacher, and S. Gombots. "Inverse Scheme for Acoustic Source Localization using Microphone Measurements and Finite Element Simulations". In: *Acta Acustica* 104 (2018), pp. 647–656.

[2] Stefan Gombots. "Acoustic source localization at low frequencies using microphone arrays". PhD thesis. TU Wien, Austria, 2020.

[3] Jonathan Nowak et al. "Inverse scheme for sound localization". In: *Tagungsband DAGA 2020*. 2020, pp. 635–638.

[4] Manfred Kaltenbacher and Sebastian Floss. "Nonconforming Finite Elements Based on Nitsche-Type Mortaring for Inhomogeneous Wave Equation". In: *Journal of Theoretical and Computational Acoustics* 26.03 (2018), p. 1850028. DOI: 10.1142/S2591728518500287.

[5] Sebastian Floss, Manfred Kaltenbacher, and Gerhard Karlowatz. "Application and Simulation of Micro-Perforated Panels in HVAC Systems". In: *10th International Styrian Noise, Vibration & Harshness Congress: The European Automotive Noise Conference*. SAE International, June 2018. DOI: https://doi.org/10.4271/2018-01-1514.

[6] M.A. Biot. "Theory of Propagation of Elastic Waves in a Fluid-Saturated Porous Solid. I. Low Frequency Range". In: *Journal of the Acoustical Society of America* 28 (1956), pp. 168–178.

[7] ASTM E2611-09. *Standard Test Method for Measurement of Normal Incidence Sound Transmission of Acoustical Materials Based on the Transfer Matrix Method*. West Conshohocken, PA: ASTM International, 2009.

[8] Yasushi Miki. "Acoustical properties of porous materials-modifications of Delany-Bazley models". In: *Journal of the Acoustical Society of Japan (E)* 11.1 (1990), pp. 19–24.

[9] Jean Allard and Noureddine Atalla. *Propagation of Sound in Porous Media: Modelling Sound Absorbing Materials*. John Wiley & Sons, 2009.

[10] Verein zur Förderung der Software openCFS. *openCFS*. 2021. URL: https://opencfs.org/ (visited on 08/24/2021).